Title
Thermoelastic displacement measured by DP-OCT for detecting vulnerable plaques.

Journal
Biomedical Optics Express, 5(2)

ISSN
2156-7085

Authors
Kim, Jihoon
Kang, Hyun Wook
Oh, Junghwan
et al.

Publication Date
2014-02-01

DOI
10.1364/boe.5.000474

Peer reviewed

Biomedical Optics EXPRESS

Thermoelastic displacement measured by DP-OCT for detecting vulnerable plaques

Jihoon Kim,[1] Hyun Wook Kang,[2,3,*] Junghwan Oh,[2,3] and Thomas E. Milner[4]

[1]*Fundamental Technology Group, Samsung-Electro Mechanics, Suwon 443-743, South Korea*
[2]*Department of Biomedical Engineering, Pukyong National University, Busan 608-737, South Korea*
[3]*Center for Marine-Integrated Biomedical Technology, Pukyong National University, Busan 608-737, South Korea*
[4]*Department of Biomedical Engineering, University of Texas at Austin, Austin, Texas 78712, USA*
[*]*wkang@pknu.ac.kr*

Abstract: The detection of thermoelastic displacement by differential phase optical coherence tomography (DP-OCT) was analytically evaluated for identifying atherosclerotic plaques. Analytical solutions were developed to understand the dynamics of physical distribution of point hear sources during/after laser irradiation on thermoelastic responses of MION-injected tissue. Both analytical and experimental results demonstrated a delayed peak displacement along with slow decay after laser pulse due to heterogeneous distribution of the point heat sources. Detailed description of the heat sources in tissue as well as integration of a scanning mirror can improve computational accuracy as well as clinical applicability of DP-OCT for diagnosing vulnerable plaque.

OCIS codes: (000.1430) Biology and medicine; (120.3890) Medical optics instrumentation; (170.4500) Optical coherence tomography; (350.5340) Photothermal effects.

References and links

1. S. C. Tyagi, "Homocysteine redox receptor and regulation of extracellular matrix components in vascular cells," Am. J. Physiol. **274**(2 Pt 1), C396–C405 (1998).
2. S. Verheye, G. R. De Meyer, G. Van Langenhove, M. W. Knaapen, and M. M. Kockx, "In vivo temperature heterogeneity of atherosclerotic plaques is determined by plaque composition," Circulation **105**(13), 1596–1601 (2002).
3. W. J. Rogers and P. Basu, "Factors regulating macrophage endocytosis of nanoparticles: implications for targeted magnetic resonance plaque imaging," Atherosclerosis **178**(1), 67–73 (2005).
4. S. Litovsky, M. Madjid, A. Zarrabi, S. W. Casscells, J. T. Willerson, and M. Naghavi, "Superparamagnetic iron oxide-based method for quantifying recruitment of monocytes to mouse atherosclerotic lesions in vivo: enhancement by tissue necrosis factor-alpha, interleukin-1beta, and interferon-gamma," Circulation **107**(11), 1545–1549 (2003).
5. M. A. Pulido, D. J. Angiolillo, and M. A. Costa, "Imaging of atherosclerotic plaque," Int. J. Cardiovasc. Imaging **20**(6), 553–559 (2004).
6. F. H. Epstein and R. Ross, "Atherosclerosis--an inflammatory disease," N. Engl. J. Med. **340**(2), 115–126 (1999).
7. P. Libby, "Inflammation in atherosclerosis," Arterioscler. Thromb. Vasc. Biol. **32**(9), 2045–2051 (2012).
8. P. Libby, "Vascular biology of atherosclerosis: overview and state of the art," Am. J. Cardiol. **91**(3), 3–6 (2003).
9. S. A. Schmitz, S. Winterhalter, S. Schiffler, R. Gust, S. Wagner, M. Kresse, S. E. Coupland, W. Semmler, and K. J. Wolf, "USPIO-enhanced direct MR imaging of thrombus: preclinical evaluation in rabbits," Radiology **221**(1), 237–243 (2001).
10. J. Oh, M. D. Feldman, J. Kim, C. Condit, S. Emelianov, and T. E. Milner, "Detection of magnetic nanoparticles in tissue using magneto-motive ultrasound," Nanotechnology **17**(16), 4183–4190 (2006).
11. J. Kim, J. Oh, T. E. Milner, and J. S. Nelson, "Imaging nanoparticle flow using magneto-motive optical Doppler tomography," Nanotechnology **18**(3), 035504 (2007).
12. S. G. Ruehm, C. Corot, P. Vogt, S. Kolb, and J. F. Debatin, "Magnetic resonance imaging of atherosclerotic plaque with ultrasmall superparamagnetic particles of iron oxide in hyperlipidemic rabbits," Circulation **103**(3), 415–422 (2001).
13. S. A. Schmitz, S. E. Coupland, R. Gust, S. Winterhalter, S. Wagner, M. Kresse, W. Semmler, and K. J. Wolf, "Superparamagnetic iron oxide-enhanced MRI of atherosclerotic plaques in Watanabe hereditable hyperlipidemic rabbits," Invest. Radiol. **35**(8), 460–471 (2000).

#194895 - $15.00 USD Received 30 Jul 2013; revised 1 Oct 2013; accepted 8 Jan 2014; published 14 Jan 2014

14. J. Barkhausen, W. Ebert, C. Heyer, J. F. Debatin, and H. J. Weinmann, "Detection of atherosclerotic plaque with Gadofluorine-enhanced magnetic resonance imaging," Circulation **108**(5), 605–609 (2003).
15. M. Sirol, V. V. Itskovich, V. Mani, J. G. Aguinaldo, J. T. Fallon, B. Misselwitz, H. J. Weinmann, V. Fuster, J. F. Toussaint, and Z. A. Fayad, "Lipid-rich atherosclerotic plaques detected by gadofluorine-enhanced in vivo magnetic resonance imaging," Circulation **109**(23), 2890–2896 (2004).
16. J. Kim, J. Oh, H. W. Kang, M. D. Feldman, and T. E. Milner, "Photothermal response of superparamagnetic iron oxide nanoparticles," Lasers Surg. Med. **40**(6), 415–421 (2008).
17. D. C. Adler, S. W. Huang, R. Huber, and J. G. Fujimoto, "Photothermal detection of gold nanoparticles using phase-sensitive optical coherence tomography," Opt. Express **16**(7), 4376–4393 (2008).
18. C. Zhou, T. H. Tsai, D. C. Adler, H. C. Lee, D. W. Cohen, A. Mondelblatt, Y. Wang, J. L. Connolly, and J. G. Fujimoto, "Photothermal optical coherence tomography in ex vivo human breast tissues using gold nanoshells," Opt. Lett. **35**(5), 700–702 (2010).
19. M. C. Skala, M. J. Crow, A. Wax, and J. A. Izatt, "Photothermal Optical Coherence Tomography of Epidermal Growth Factor Receptor in Live Cells Using Immunotargeted Gold Nanospheres," Nano Lett. **8**(10), 3461–3467 (2008).
20. B. Bonnemain, "Superparamagnetic agents in magnetic resonance imaging: physicochemical characteristics and clinical applications. A review," J. Drug Target. **6**(3), 167–174 (1998).
21. C. M. Pitsillides, E. K. Joe, X. Wei, R. R. Anderson, and C. P. Lin, "Selective cell targeting with light-absorbing microparticles and nanoparticles," Biophys. J. **84**(6), 4023–4032 (2003).
22. T. Akkin, D. P. Davé, J. I. Youn, S. A. Telenkov, H. G. Rylander 3rd, and T. E. Milner, "Imaging tissue response to electrical and photothermal stimulation with nanometer sensitivity," Lasers Surg. Med. **33**(4), 219–225 (2003).
23. D. P. Davé and T. E. Milner, "Optical low-coherence reflectometer for differential phase measurement," Opt. Lett. **25**(4), 227–229 (2000).
24. K. Seo and T. Mura, "The Elastic Field in a Half Space Due to Ellipsoidal Inclusions With Uniform Dilatational Eigenstrains," J. Appl. Mech. **46**(3), 568–572 (1979).
25. J. H. Davies, "Elastic Field in a Semi-Infinite Solid due to Thermal Expansion or a Coherently Misfitting Inclusion," J. Appl. Mech. **70**(5), 655–660 (2003).
26. R. D. Mindlin and D. H. Cheng, "Thermoelastic Stress in the Semi-Infinite Solid," J. Appl. Mech. **21**, 931–933 (1950).
27. J. N. Goodiee, "XCVII. On the integration of the thermo-elastic equations," in *Philosophical Magazine Series 7*(Taylor & Francis, 1937), pp. 1017–1032.
28. S. Liu, M. J. Rodgers, Q. Wang, and L. M. Keer, "A Fast and Effective Method for Transient Thermoelastic Displacement Analyses," J. Tribol. **123**(3), 479–485 (2001).
29. L. Yu, M. Huang, M. Chen, W. Chen, W. Huang, and Z. Zhu, "Quasi-discrete Hankel transform," Opt. Lett. **23**(6), 409–411 (1998).
30. M. Guizar-Sicairos and J. C. Gutiérrez-Vega, "Computation of quasi-discrete Hankel transforms of integer order for propagating optical wave fields," J. Opt. Soc. Am. A **21**(1), 53–58 (2004).
31. F. D. Kolodgie, A. S. Katocs, Jr., E. E. Largis, S. M. Wrenn, J. F. Cornhill, E. E. Herderick, S. J. Lee, and R. Virmani, "Hypercholesterolemia in the rabbit induced by feeding graded amounts of low-level cholesterol. Methodological considerations regarding individual variability in response to dietary cholesterol and development of lesion type," Arterioscler. Thromb. Vasc. Biol. **16**(12), 1454–1464 (1996).
32. R. Weissleder, J. F. Heautot, B. K. Schaffer, N. Nossiff, M. I. Papisov, A. Bogdanov, Jr., and T. J. Brady, "MR lymphography: study of a high-efficiency lymphotrophic agent," Radiology **191**(1), 225–230 (1994).

1. Introduction

Atherosclerosis is a coronary artery disease with high mortality rate that is mainly caused by rupture of vulnerable plaque. The disease can be represented by a hardening of arteries [1], variations in arterial temperature [2], and a chronic buildup of plaque [3]. As a result, constriction of blood vessels and reduced blood supply to tissue can lead to myocardial infarction [4]. Coronary angiography has been used for 40 years as a major imaging modality to detect atherosclerosis [5]. However, the detection of the vulnerable plaques still requires a diagnostic tool that can provide molecular and cellular information on the risk of rupture along with anatomical changes of the blood vessels mainly due to the lack of correlation between narrowing lumen and rupture of the vulnerable plaque. Macrophage has been acknowledged as an early cellular marker of the plaque rupture as it can induce the breakdown of a thin fibrous cap in the vessel. Thus, the detection of the macrophage has been clinically pivotal in identifying the location of the vulnerable plaque as well as determining the progression of atherosclerosis [6–8].

Ultrasmall superparamagnetic iron oxide nanoparticles (USPION) have demonstrated a capability of detecting inflammatory activity of atherosclerotic plaques in light of uptake by

#194895 - $15.00 USD Received 30 Jul 2013; revised 1 Oct 2013; accepted 8 Jan 2014; published 14 Jan 2014

macrophages [9]. The nanoparticles can be combined with other imaging modalities such as optical coherence tomography, optical doppler tomography, and ultrasound for lesion identification [4,10,11]. Among various imaging modalities, magnetic resonance imaging (MRI) has often been used to detect inflammation in the atherosclerotic plaques with the aid of the intravenously injected-USPION [3,4,12,13]. The principle was to estimate the potential location of the plaque where the macrophages engulf the nanoparticles. However, in spite of the increased contrast and feasible detection of USPION-phagocytosed plaques, the MRI technique still presented inherently low sensitivity and contrast-to-noise ratio and hardly characterized the atherosclerotic plaques [14]. In addition, the magnetic iron oxide nanoparticles can hardly be delivered to the targeted atherosclerotic plaque via blood stream, in that most of the particles are typically taken up by major phagocytic systems (MPS) such as liver and spleen [12,13]. Thus, the modality is still difficult to complete the detection of high-risk plaques [15].

Another approach can involve the use of absorptive gold nanoparticles or monocrystallin iron oxide nanoparticles (MION) in conjunction with laser excitation for photothermal detection [16–19]. Particularly, MION is FDA-approved nanoparticles for MRI applications, which are small enough to escape form MPS and reach the macrophages existing inside the atherosclerotic plaque [20]. It was reported that MION could selectively absorb the 532 *nm* wavelength, inducing temperature increase in tissue [16]. Since the resultant photothermal response typically leads to thermoelastic movement of the MION-laden tissue, measurements of both surface displacement and laser-induced temperature were implemented for detection of non-cardiovascular diseases [21]. In order to detect micro-displacement of MION-injected tissue, differential phase optical coherence tomography (DP-OCT) can be a feasible tool, in that DP-OCT can measure the optical path length changes in tissue with high phase sensitivity and resolution [22,23]. However, the physical distribution and delivered concentration of MION in tissue are still poorly understood, so it is difficult to predict the thermal behaviors of the nanoparticles particularly for the potential detection of atherosclerotic plaques. In addition, no analytical approach has been performed to specifically investigate the feasibility of DP-OCT in association with the displacement of MION for cardiovascular applications.

To understand thermoelastic responses of nanoparticles to laser irradiation for the feasible atherosclerotic detection, the current study developed analytical models and evaluated various thermal conditions of the nanoparticles in tissue. Primarily, a two-step approach was applied to gradually increase the complexity of the analytical solution for thermoelastic surface displacement. The model was initially developed with a single point heat source and then expanded to distributed point heat sources, which could be more relevant to the MION-induced temperature distribution in tissue. For model validation, MION-injected arterial tissue was prepared and irradiated with 532 *nm* laser light for thermal excitation *ex vivo* and simultaneously detected by DP-OCT to measure the laser-induced optical path length changes in the MION-laden tissue due to thermoelastic responses.

2. Theoretical analysis

Thermoelastic displacement due to non-uniform temperature distribution in a semi-infinite half space has been of great interest in previous studies [24,25]. An analytical solution proposed by Mindlin and Cheng can then be used to describe the thermoelastic displacement of nanoparticle-embedded media [26]. Firstly, elastic potential of sources in a semi-infinite body ($z > 0$) that is assumed to be free of traction at the surface can be derived by applying image sources ($z < 0$) and their derivatives for the elastic field (u) at a center of dilatation.

$$u = -\frac{1}{4\pi}\left(\nabla\varphi + \nabla_2\varphi_2\right) \tag{1}$$

#194895 - $15.00 USD Received 30 Jul 2013; revised 1 Oct 2013; accepted 8 Jan 2014; published 14 Jan 2014

where φ and φ_2 are each elastic potential of a point heat source in a semi-infinite half space and in the image space respectively. In addition, ∇_2 in Eq. (1) can be defined as follows:

$$\nabla_2 = (3-4\nu)\nabla + 2\nabla z(\partial/\partial z) - 4(1-\nu)\hat{k}\nabla^2 z \quad (2)$$

where v is Poisson's ratio and $\hat{k}$ is a unit vector in *z*-direction (depth). The elastic potentials (φ and φ_2) are the integral of the distribution of a dilatation center in a volume of interest [27]. The current analysis attempted to solve a thermoelastic surface displacement, $u_3(x, y, 0)$, where the subscript 3 means the direction of displacement normal to the surface, induced by a point heat source representing a single MION particle engulfed by macrophages at (0, 0, *c*), where *c* indicates a depth of the point heat source in a semi-infinite half space ($0 < z < \infty$) with an insulating boundary. Accordingly, two analytical solutions were derived and developed: the thermoelastic displacement due to the instantaneous heating of a point heat source (Fig. 1(a)) and a group of point heat sources (Fig. 1(b)).

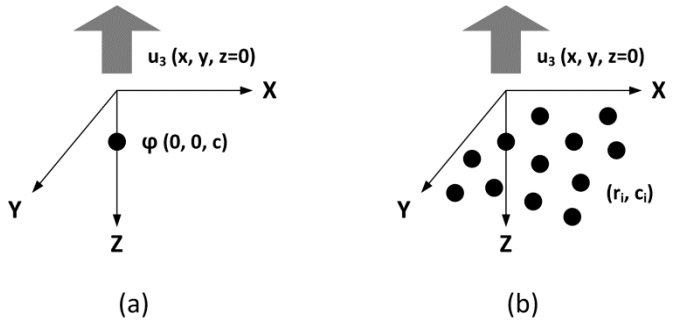

Fig. 1. Surface displacement of semi-infinite half space insulating from point elastic potential: (a) thermoelastic displacement due to instantaneous heating of point heat source and (b) group of point heat sources

A point heat source can result in a temperature increase, $\Delta T(\hat{\xi}, t)$, where $\hat{\xi}$ represents a position vector in Cartesian coordinates for the point heat source located along the *z*-axis at (0, 0, *c*) in a semi-infinite half space and *t* (*sec*) is time. Seo and Mura solved an analytical solution for the thermoelastic displacement caused by an inclusion that has uniform dilatational eigen strains, $\varepsilon^*(\hat{\xi}, t)$, in a semi-infinite half space [24]. Thus, $\varepsilon^*(\hat{\xi}, t)$ can be replaced by a linear thermal expansion, $\alpha \cdot \Delta T(\hat{\xi}, t)$, where α (*m*/*K*) is a linear thermal expansion coefficient, in consideration of the semi-infinite half space when the surface plane is free of traction [25]. Liu *et al.* used Seo and Mura's approach to derive an integral equation for a thermoelastic displacement in the half-space with arbitrary temperature distribution [28]. Consequently, the integral expression for the normal surface displacement $u_3(x, y, z = 0, t)$ at lateral position (*x*, *y*) and time *t* is as follows:

$$u_3(x, y, 0, t) = \frac{-\alpha(1+\nu)}{\pi} \int_0^{\infty} \int_{-\infty}^{\infty} \int_{-\infty}^{\infty} \Delta T(\hat{\xi}, t) \times \frac{\xi_3}{\left((x-\xi_1)^2 + (y-\xi_2)^2 + \xi_3^2\right)^{3/2}} d\xi_1 d\xi_2 d\xi_3 \quad (3)$$

A temperature increase ($\Delta T(\hat{\xi}, t)$) due to the instantaneous heating of a point heat source in a semi-infinite media with an insulating boundary condition can be written as a sum of two Green's functions;

#194895 - $15.00 USD Received 30 Jul 2013; revised 1 Oct 2013; accepted 8 Jan 2014; published 14 Jan 2014

$$\Delta T\left(\hat{\xi},t\right)=\frac{1}{8\left(\pi Dt\right)^{3/2}}\frac{Q}{\rho\cdot C_p}\exp\left(-\frac{\left(c^2+\xi_1^{\,2}+\xi_2^{\,2}+\xi_3^{\,2}\right)}{4Dt}\right)\cos\mathrm{h}\left(\frac{\xi_3\cdot c}{2Dt}\right) \qquad (4)$$

where ρ (K/mm^3) is density, C_p ($kJ/Kg{\cdot}K$) heat capacity, Q (J) laser energy, and D (mm^2/s) thermal diffusivity. Then, $\Delta T(\hat{\xi},t)$ in Eq. (3) can be substituted into Eq. (4) as follows:

$$\begin{aligned}u_3\left(x,y,0,t;(0,0,c)\right)=&\frac{-\alpha(1+\nu)}{4\pi\left(\pi Dt\right)^{3/2}}\frac{Q}{\rho\cdot C_p}\exp\left(-\frac{c^2}{4Dt}\right)\int_0^\infty\cos\mathrm{h}\left(\frac{\xi_3\cdot c}{2Dt}\right)\exp\left(-\frac{\xi_3^{\,2}}{4Dt}\right)d\xi_3\\&\times\int_{-\infty}^{\infty}\int_{-\infty}^{\infty}\frac{\xi_3}{\left((x-\xi_1)^2+(y-\xi_2)^2+\xi_3^{\,2}\right)^{3/2}}\exp\left(-\frac{\left(\xi_1^{\,2}+\xi_2^{\,2}\right)}{4Dt}\right)d\xi_1 d\xi_2\end{aligned} \qquad (5)$$

where (0, 0, c) is the location of the heat source.

A Hankel transform (HT) can then be applied to Eq. (5) in order to simplify integrals ξ_1 and ξ_2 by transforming a space (r) domain displacement into the corresponding spatial frequency ($k=\sqrt{k_1^2+k_2^2}$) [29]. The thermoelastic displacement in the spatial frequency domain (k) can be expressed as follows:

$$u_3\left(k,0,t;(0,c)\right)=\frac{-\alpha(1+\nu)Q}{\rho\cdot C_p}\left[\begin{array}{l}\exp\left(-2\pi kc\right)erfc\left(2\pi k\sqrt{Dt}-c/2\sqrt{Dt}\right)\\+\exp\left(2\pi kc\right)erfc\left(2\pi k\sqrt{Dt}+c/2\sqrt{Dt}\right)\end{array}\right] \qquad (6)$$

where (0, c) is the location of the point heat source in a cylindrical coordinate and k is a spatial frequency. Then, the normal surface displacement in a space (r) domain can be obtained by using the inverse Hankel transform (IHT). However, as no analytical solution for IHT has been found, a quasi-discrete numerical Hankel transform [29] modified by Guizar-Sicairos *et al.* was applied instead, and their numerical solution was adapted to obtain the thermoelastic surface displacement (u_3) in the space domain [30].

$$u_3\left(r,0,t;(0,c)\right)=IHT\left[u_3\left(k,0,t\right)\right]=\int_0^\infty 2\pi\cdot u_3\left(k,0,t\right)\cdot J_o\left(2\pi kr\right)k\,dk \qquad (7)$$

where $J_o\left(r\right)$ is the zero-order Bessel function [29].

For thermoelastic surface displacement of a point heat source (0, 0, c) during pulse duration (t_p), the time-integral of the displacement due to instantaneous heating can be computed.

$$u_3\left(r,0,t\le t_p;(0,c)\right)=IHT\left[\frac{-\alpha(1+\nu)}{\rho\cdot C_p}\int_0^t\dot{Q}\left\{\begin{array}{l}\exp\left(-2\pi kc\right)erfc\left(2\pi k\sqrt{Dt'}-c/2\sqrt{Dt'}\right)\\+\exp\left(2\pi kc\right)erfc\left(2\pi k\sqrt{Dt'}+c/2\sqrt{Dt'}\right)\end{array}\right\}dt'\right] \qquad (8)$$

where $\dot{Q}$ [J/s] is the delivery rate of laser energy (i.e. laser energy per time). At a time after t_p, an integral for the thermoelastic surface displacement can be obtained by replacing t' with $t-t'$ in Eq. (9).

$$u_3\left(r,0,t>t_p;(0,c)\right)=IHT\left[\frac{-\alpha(1+\nu)}{\rho\cdot C_p}\int_0^t\dot{Q}\left\{\begin{array}{l}\exp\left(-2\pi kc\right)erfc\left(2\pi k\sqrt{D(t-t')}-c/2\sqrt{D(t-t')}\right)\\+\exp\left(2\pi kc\right)erfc\left(2\pi k\sqrt{D(t-t')}+c/2\sqrt{D(t-t')}\right)\end{array}\right\}dt'\right] \qquad (9)$$

#194895 - $15.00 USD Received 30 Jul 2013; revised 1 Oct 2013; accepted 8 Jan 2014; published 14 Jan 2014

Finally, atherosclerotic tissue contains a number of macrophages, which engulf a great deal of MION. In order to reflect the MION aggregation, the impact of multiple point heat sources was analyzed (Fig. 1(b)). The thermoelastic displacement of the point heat sources distributed in a semi-infinite half space can be expressed by a linear superposition of the thermoelastic displacements induced by each point heat source as follows;

$$u_3^D\left(r,\,0,\,t;(b_i,c_i)\right)=\sum_{i=1}^{N}u_3^p\left(r,\,0,\,t;(b_i,c_i)\right) \tag{10}$$

where the superscripts D and p represents the distribution of the entire point heat sources and laser heating during the pulse duration.

3. Experiments

As a superparamagnetic intravascular contrast agent, MION was used for the current model validation. The absorption spectra of MION (total diameter of 30 *nm* including dextran coating along with core diameter of 4~7 *nm*) were preliminarily evaluated to enable the detection of atherosclerotic vulnerable plaque *ex vivo* [16]. For the *ex vivo* experiments, a rabbit model was used to create atherosclerotic plaques in the aorta [31]. The animal protocol was approved by the Institutional Animal Care and Use Committee (IACUC) at the University of Texas Health Science Center at San Antonio. Two Watanabe heritable hyperlipidemic (WHHL) rabbits (ages of 1-2 years) were harbored to have plaque formation within the aortic wall. A WHHL rabbit was sedated with inhaled Halothane, and 2.96 *ml* of MION (concentration = 200 *mmol Fe/kg* [32]) was administered into the marginal vein of the rabbit ear prior to the *in vitro* tests. For a control WHHL rabbit, 2 *ml* of saline was injected instead. Three days after intravenous injection, the rabbits were euthanized with a lethal dose of phenobarbitol after sedation with inhaled isoflurane, and 2 *ml* of heparin was injected to prevent blood clotting. Thoracic and abdominal aorta were extracted from each rabbit and perfused with saline to remove any blood contamination. Prior to tissue excision, the medical doctors at the center visually identified and confirmed the atherosclerotic plaque formed in the blood vessel. Then, segments of the aortas were prepared in size of 4×4 mm^2 for control and MION-accumulated samples (N = 4 for each group), and they were stored at 4 $^{\circ}C$ in saline before use to minimize any dehydration and morphological changes.

Pulsed laser light (wavelength = 532 *nm*, pulse duration = 100 *ms*, fluence rate = 2.26 W/cm^2) was applied through a 400-μm core fiber to generate thermoelastic responses of MION in aortic tissue (Fig. 2). A DP-OCT system with near-IR light ($\lambda = 1.31 \pm 60$ μm, AFC Technologies Inc., Hull, Quebec, Canada) was employed to measure surface displacements in tissue in response to the laser irradiation with a phase sensitivity of ~10^{-3} *rad* and the minimum detectable optical path length change of ~0.2 *nm* [22,23]. The DP-OCT system principally consisted of polarization-maintained fibers and two different orthogonal polarized lights (// and $\times$) that traveled in the system with a time-delay due to the insertion of a calcite prism in a sample arm (Fig. 2(a)). Each polarized light was reflected from an interface where refractive index difference existed and caused the resultant interference in the system. In turn, DP-OCT measured the optical path length change at a nanometer scale by calculating the differential phase between two of these polarized lights, reflected from the sites of interest.

During experiments, each tissue sample was placed on top of a base plate at room temperature and fixed in between two microscope slides with 3 mm spacers situated as shown in Fig. 2(b). The potential area of plaque formation on the inner arterial wall was exposed to DP-OCT beam to measure thermoelastic displacements. The wall surface was flattened out to have minimal spatial variations of IR emission during laser irradiation. For the current setup, two back-scattered lights from a glass-air interface and an air-artery interface respectively were detected to measure the surface displacement of the tissues. Thus, the thermoelastic displacements were compared between MION-injected and control WHHL rabbit arteries in

#194895 - $15.00 USD Received 30 Jul 2013; revised 1 Oct 2013; accepted 8 Jan 2014; published 14 Jan 2014

light of optical path length variations. All the preparation and experiments were completed within 6 *h* after animal euthanasia. No statistical difference between the animals was reflected in the current study.

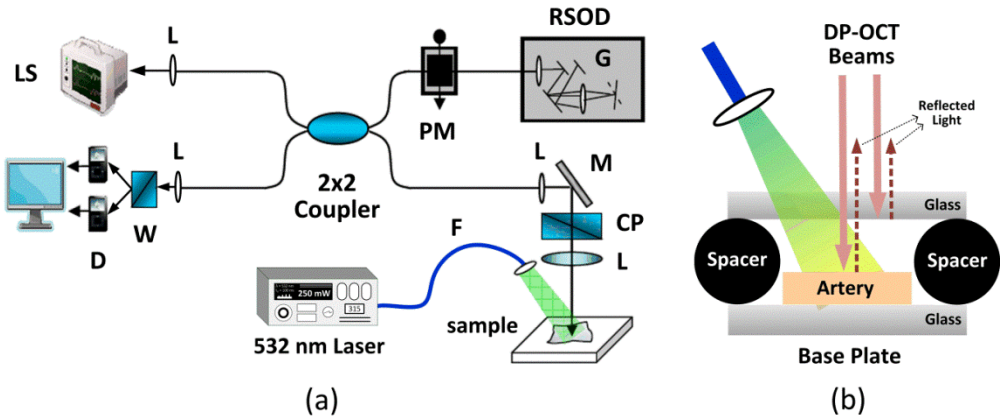

Fig. 2. Measurement of thermoelastic displacements induced by 532-*nm* laser irradiation: (a) DP-OCT setup consisting of optical semiconductor amplifier light source (LS), lens (L), rapid scanning optical delay (RSOD) line, phase modulator (PM), mirror (M), calcite prism (CP), grating, (G), detector (D), and Wollaston prisms (W) and (b) detailed description of sample geometry indicating two separated locations (glass-air and air-artery boundaries)

4. Results and discussion

The developed analytical solutions were utilized to explore the thermal responses of nanoparticles to pulsed laser irradiation under various conditions. Initially, the impact of a single point heat source (i.e. single MION) on thermoelastic surface displacement was investigated in terms of spatial distribution of the source (axial and radial positions). Assuming that a DP-OCT detection point was fixed at the origin (0, 0, 0), the physical locations of the heat source relative to the detection point were varied to explore thermal responses of the MION-injected tissue during and after laser irradiation. Figure 3(a) presents variations in normalized surface displacements as a function time for four axial positions (i.e. 50, 100, 150, and 200 μm) from the detection point (0, 0, 0) and a fixed radial position ($r = 0$) under 50 *ms* laser irradiation. Overall, the displacement initially increased during pulse duration but sharply decreased after the pulse. The maximum displacement occurred at the end of the pulse duration and almost linearly decreased with increasing the axial positions. According to the current model, the sharp decay in the thermoelastic displacement after 50 *ms* implicates that the surface displacement was influenced primarily by the heat source along the depth axis. Regardless of the axial position, the equivalent decay rates after the pulse occurred possibly due to the absence of point heat sources that were laterally located in tissue. In addition, in spite of the fixed detection point, the surface displacements at deeper locations were still computable, in that the direction of the thermal wave propagation could remain identical (i.e. normal to the tissue surface).

Figure 3(b) exhibits the effect of radial positions of a point heat source on thermoelastic surface displacements. In the model, the depth of a point heat source was fixed at 5 μm, and the heat source was located at various radial positions (i.e. 0, 63, 96, and 129 μm). Similarly, the surface displacement initially increased during the pulse duration but sharply decreased upon termination of the pulse. However, it was noted that after the pulse, the displacement gradient significantly decreased with increasing the radial positions. Unlike Fig. 3(a), the peak displacement also decreased more rapidly with the radial positions away from the detection point. Therefore, from the fixed detection point, the lateral location of the heat source determined not only the magnitude of the displacement as well as the gradient of the

#194895 - $15.00 USD Received 30 Jul 2013; revised 1 Oct 2013; accepted 8 Jan 2014; published 14 Jan 2014

thermoelastic responses in tissue whereas the axial position of the point heat source solely affected the magnitude of the thermoelastic displacement.

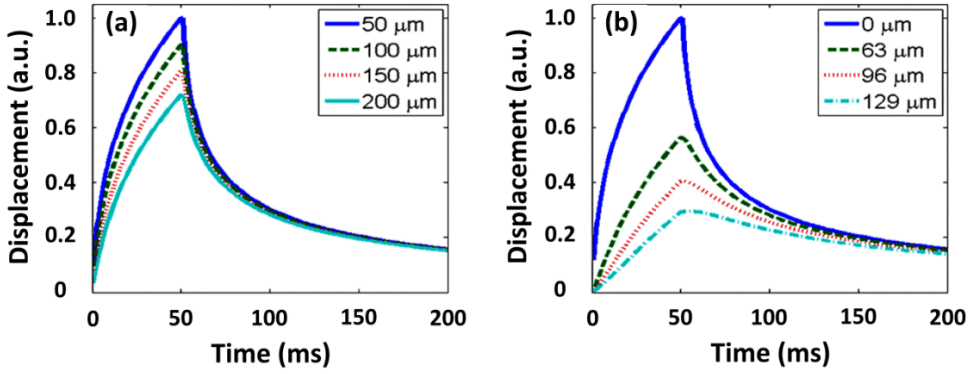

Fig. 3. Simulation results of normalized thermoelastic surface displacement due to pulsed heating (pulse duration = 50 *ms*) of point heat source in semi-infinite medium at (a) various depths with fixed radius (r = 0, origin) and (b) various radial positions away from detection point at fixed depth (z = 5 μm)

Next, thermoelastic responses of MION-injected tissue were evaluated in consideration of a group of point heat sources. As aforementioned, multiple heat sources were constructed by a superposition of the thermoelastic displacement due to an individual point heat source. Since MION can be haphazardly distributed in arterial tissue, two possible distributions of a group of the point heat sources were considered: (a) homogenous and (b) heterogeneous distribution of point heat sources. Particularly, for the latter case, the position of the detection area would be pivotal in determining strength and tendency of the thermoelastic responses in tissue, in that the current DP-OCT system was based upon single-point detection. Thus, as validated in Fig. 3, two different scenarios were applied: (a) detection of displacement immediately above MION and (b) detection of displacement radially distant from MION. For the sake of simplicity, the macrophages engulfing MION were assumed to be located within the irradiated area. Figure 4 demonstrates three cases of the surface displacements during and after 100 *ms* laser irradiation that were normalized for the purpose of direct comparison. Figure 4(a) represents the homogeneous distribution (every 5 μm interval) of a group of the point heat sources within a heated volume (35 μm in depth by 50 μm in radius) below the detection point, assuming that light penetration was smaller than the diameter of the heated area. The profile showed a faster increase of surface displacement due to rapid temperature increase and the dramatic decay with the time constant of approximately 110 *ms* after the pulse. In the face of the superposition of multiple surface displacements due to heat diffusion from the surrounding heat sources, the surface displacements directly below the detection point were found to be higher than other areas. The current findings were also consistent with our previous study with a solution of MION, representative of a homogeneous medium [16]. Therefore, under the homogeneous distribution, the overall shape of the thermoelastic surface displacements can be mainly determined by a group of the heat sources close to the detection point.

Figures 4(b) and 4(c) represent the heterogeneous distribution of MION detected by DP-OCT above and away from MION respectively. Unlike Fig. 4(a), both cases showed a slower decay of the thermoelastic surface displacement after laser pulse. It is hypothesized that the significant thermal diffusion from the peripheral heat sources into the detection point compromised the decay of the thermoelastic displacements due to heterogeneity of the MION-distribution in tissue. It was also noted that the detection point remote from the sources contributed to continuous increase of the displacement even around 100 *ms* after the laser pulse. Thus, the peak surface displacement occurred at around 200 *ms* after the onset of

#194895 - $15.00 USD Received 30 Jul 2013; revised 1 Oct 2013; accepted 8 Jan 2014; published 14 Jan 2014

the pulse whereas the other cases generated the peak displacement at the end of the pulse. Conceivably, the delayed displacement implicates that the heat influx originated from the heterogeneous heat sources took time to be transferred to the detection point. Then, thermal energy could be continuously accumulated and expanded to the detection point, which was faster than heat loss. However, the absolute magnitude of the displacement in Fig. 4(c) was found to be up to 50% smaller than the other cases as the signal strength notably diminished during the thermal wave propagation to the detection point.

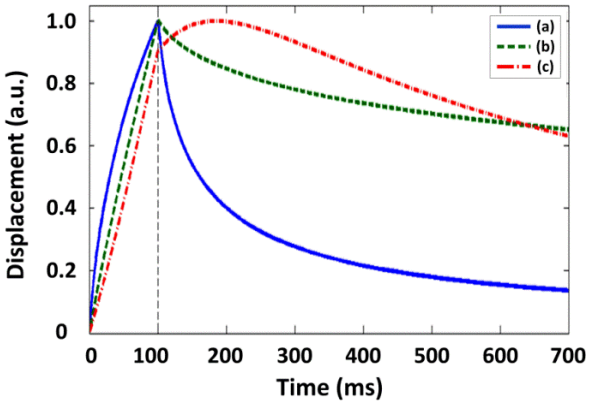

Fig. 4. Simulation of normalized thermoelastic displacements due to pulsed laser irradiation (100 *ms* duration) in semi-infinite medium: (a) homogeneously distributed point heat sources with 5 μm intervals, (b) heterogeneously distributed heat sources with detection point above group of heat sources, and (c) heterogeneously distributed sources with detection point 300-μm distant from group of heat sources

Figure 5 presents the thermoelastic surface displacements of rabbit arteries in response to laser irradiation experimentally measured by DP-OCT. The existence and location of MION in arterial tissue was histologically investigated in a previous study [10]. Both RAM-11 and Prussian Blue positive staining localized macrophages as well as iron of the engulfed MION, which were located near the luminal surface of the intimal hyperplasia. The histological findings ostensibly evidenced that macrophages in atherosclerotic plaques could engulf the nanoparticles following intravenous injection of MION. Overall, both MION-injected and control tissues initially generated rapid increase of surface displacements during and around 20 *ms* after the pulse duration. The displacements, however, decreased gradually with time due to temperature decrease by heat diffusion to the peripheral tissue. In the case of the MION-injected tissue, the thermoelastic displacement reached up to 1270 *nm* with the increase rate of 11.0 *nm*/*ms*, which was 3.2 fold in comparison with the control. Accordingly, the faster increase of the displacement evidenced that selective light absorption by MION can be a strong indication of atherosclerotic plaques, which can evidently be detected by DP-OCT. Due to the faster heat deposition by MION in tissue, the thermal decay rate was approximately 0.9 *nm*/*ms* upon termination of the pulse. On the other hand, the control tissue showed a slower increase of the surface displacement reaching only up to 400 *nm* (i.e. 3.5 *nm*/*ms*). Less heat accumulation caused a lower gradient of displacement decrease down to 0.02 *nm*/*ms*. It can be conceived that the residual chromophores such as erythrocytes and blood vessels contributed to temperature increase upon light absorption in spite of absence of MION in control tissue. Still, the degree of thermoelastic response from the control would be quite insufficient for DP-OCT detection in light of clinical applications.

#194895 - $15.00 USD Received 30 Jul 2013; revised 1 Oct 2013; accepted 8 Jan 2014; published 14 Jan 2014

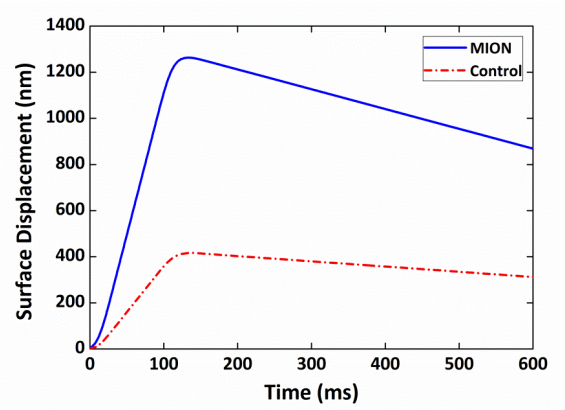

Fig. 5. Thermoelastic surface displacements of rabbit arteries in response to 532-*nm* pulsed laser irradiation (100 *ms* duration)

In terms of the delayed peak displacement and slow decay, the experimentally observed thermoelastic surface displacement from MION-laden tissue (Fig. 5) was largely comparable to the analytical solution shown in Fig. 4(c). The continuous increase of the measured thermoelastic surface displacement after the pulse implies that the number of MION-engulfed macrophages under the detection point was smaller than that of macrophages distant from the detection point. Thus, the heated macrophages, which were located distant from the detection point of DP-OCT, resulted in the delayed increase of the displacement even after the pulse and a slower decrease of the thermoelastic displacement as shown Fig. 4(c). These results are consistent with the histologic locations of both macrophages and engulfed MION in our previous study [10]. However, in spite of the comparable decay rate, the peak displacement in Fig. 5 was reached five times fast as that in Fig. 4(c), possibly resulting from low density of MION near the detection point. Thus, the increase rate of the peak surface displacement can be determined primarily by the number of heat sources away from the detection point.

The current study presented that photothermal detection of surface displacements to identify atherosclerotic macrophages was solely based upon the selective heating of absorptive nanoparticles (MION) in a MION-laden vulnerable plaque and their photothermal responses. Although the 3:1 difference in surface displacements between MION-laden and unladen atherosclerotic tissue was appreciated in Fig. 5, it should be noted that the "contrast ratio" could substantially decrease or vanish when comparing a MION-laden vulnerable plaque with below-average macrophage content or below-average MION uptake to a MION-laden normal artery with above-average thermal absorption or MION uptake. Thus, further investigations should be conducted to differentiate normal from pathologic atherosclerotic tissue in light of macrophage content as well as MION uptake or thermal absorption in the macrophages. In addition, more histopathological understanding of MION concentration as well as distribution in tissue should be performed to improve the accuracy of the current computation. In spite of a comparable development of the surface displacement, incorporation of more detailed information on heat source distribution into the current model will be able to determine the threshold of the surface displacement for detection, the optimal concentration of the nanoparticles, and the appropriate selection of both various nanoparticles (i.e. non-superparamagnetic) and excitation wavelengths (i.e near-IR for deep optical penetration). Furthermore, it is notable that the current model took into account optical path length changes dominated merely by physical thermal expansion without consideration of variations in tissue refractive index. In fact, our previous study found that the thermal expansion affected the overall optical path length change significantly (more than ten times), in comparison with the refractive index [16]. However, in order to enhance the accuracy of the numerical simulation,

#194895 - $15.00 USD Received 30 Jul 2013; revised 1 Oct 2013; accepted 8 Jan 2014; published 14 Jan 2014

the future study will incorporate the effect of thermal change in refractive index in tissue into the current analytical model.

In an attempt to validate the current findings, the follow-up *in vivo* studies are presently under consideration. However, several challenges should be deliberated in association with translation to the *in vivo* application. For instance, as intravascular OCT typically requires a contrast flush to clear blood from the targeted vessel during imaging, the flush would act as a cooling mechanism to diffuse heat away from the tissue, leading to the considerable attenuation of the surface displacement effects. Next, cardiac and respiratory actions would induce gross vessel motions, which could make it challenging to reliably detect sub-micron surface displacements during the *in vivo* testing. Finally, the compliance in the media, adventitia, and epicardial tissues would partially diminish the path changes, in that an intact, functioning artery could expand differently, in comparison with the excised tissue used in the current study. Therefore, the inherent anatomical and physiological challenges should be addressed and thoroughly resolved to achieve favorable outcomes from the *in vivo* use.

Although the current analytical results showed a good agreement with the experimental measurements, there are still a number of technical limitations to overcome for clinical applications. Firstly, as DP-OCT was associated with single-point detection, repetitive identification processes of MION were performed during the experiments. In order to reduce the identification time and to explore the sites of interest promptly, the addition of a scanning mirror to the current DP-OCT system is underway. Accordingly, high sensitivity as well as increased mobility can enable the system to be more clinically applicable. Next, the thermoelastic surface displacement of the arterial tissue will be confirmed with a thermal IR camera to correlate temperature increase with thermoelastic expansion and to validate the current computational model in terms of peak displacement as well as its decay gradient. Finally, for clinical translation, it may be advantageous to integrate optical fiber-based excitation and detection methods into a single delivery device to providing the real-time feedback for detecting atherosclerotic plaques in tissue.

5. Conclusion

The current study developed an analytical model to understand thermoelastic surface displacements of MION-injected arterial tissue in response to pulsed laser heating. Both single and group of point heat sources demonstrated the dependence of the surface displacement on MION distribution. The experimental measurements validated the analytical solution in terms of heterogeneous distribution of the point heat sources in association with distant DP-OCT detection. The current model can be used to determine the signal threshold and to optimize nanoparticle concentration for plaque detection by exploring more precise distribution of the heat sources in tissue. However, the further comparative experiments in terms of macrophage content and MION uptake should be performed to evaluate the detectability of DP-OCT to specify the photothermal response of the MION-laden tissue. Addition of a scanning mirror to current DP-OCT systems as well as development of fiber-based multimodal approaches are also underway to enhance the clinical applicability of vulnerable plaque detection. The detection of the thermoelastic surface displacement by DP-OCT could be a feasible diagnostic tool to perform cellular monitoring macrophage-based plaque.

Acknowledgments

The authors appreciate Dr. Feldman at the University of Texas Health Science Center at San Antonio for animal preparation and tissue handling.

#194895 - $15.00 USD Received 30 Jul 2013; revised 1 Oct 2013; accepted 8 Jan 2014; published 14 Jan 2014